

Detection of Moving Objects in Earth Observation Satellite Images

ERIC KETO¹ AND WESLEY ANDRÉS WATTERS²

¹*Harvard University, Institute for Theory and Computation
60 Garden Street, Cambridge, MA USA*

²*Wellesley College, Whitin Observatory
106 Central St., Wellesley, MA 02481, USA*

ABSTRACT

Moving objects have characteristic signatures in multi-spectral images made by Earth observation satellites that use push broom scanning. While the general concept is applicable to all satellites of this type, each satellite design has its own unique imaging system and requires unique methods to analyze the characteristic signatures. We assess the feasibility of detecting moving objects and measuring their velocities in one particular archive of satellite images made by Planet Labs Corporation with their constellation of SuperDove satellites. Planet Labs data presents a particular challenge in that the images in the archive are mosaics of individual exposures and therefore do not have unique time stamps. We explain how the timing information can be restored indirectly. Our results indicate that the movement of common transportation vehicles, airplanes, cars, and boats, can be detected and measured.

Keywords: METHODS: DATA ANALYSIS, TECHNIQUES: IMAGE PROCESSING

1. INTRODUCTION

Satellites that survey large areas of the earth generally collect single-frame images rather than full-motion video. Nonetheless, the motion of observed objects creates characteristic signatures in single-frame images obtained by push broom scanning. In this technique, if the regions on the camera's sensor that are responsible for the different spectral bands are arranged as stripes perpendicular to orbital track, then the spectral images are observed at slightly different times as the orbital velocity pushes the camera over the area imaged. The spectral images represent a video with a frame rate equal to the transit time and a duration set by the number of spectral bands. If the time scale of the motion of an imaged object is commensurate with the transit time of the satellite, the moving object appears at a different location in the images in different spectral bands. In the difference of the images in two spectral bands, a moving object appears as a positive and negative pair. A second signature of motion results from the different colors of the spectral band images. In a full-color composite, the moving object appears as displaced ghosts in different colors. Both effects depend on the velocity of the moving object with respect to the velocity of the satellite and also on the characteristics of the imaging system.

Here we explore the feasibility of identifying and characterizing moving objects in one archive of Earth observation images made by Planet Labs Corporation with their latest constellation of satellites named SuperDove (Planet Labs Corporation 2021). These satellites image in seven spectral bands in the optical and one in the near infrared. Our results show that objects moving with speeds of typical transportation vehicles, cars, boats, and aircraft, are easily detectable by eye. The minimum ($\sim 20 \text{ ms}^{-1}$) detectable ground speeds is set by the spatial resolution. There is an ambiguity between the speed and altitude of an object that is discussed further in section §5.1.

Other studies have exploited timing differences in satellite images to detect motion. The procedures used are specific to each satellite. For example, the Quickbird satellite imaged the same scene in black and white and color with an 0.2 s delay that allows detection of motion (Easson et al. 2010). Heiselberg (2019); Heiselberg & Heiselberg (2021) used the same general technique adapted to images from the multispectral Sentinel-2 satellite. Here we restrict our study to the data taken by Planet Labs SuperDove satellites although our discussion is applicable more generally to satellites with similar imaging characteristics.



Figure 1. Composite visual image from the Planet Labs data set 20220530_173806_19_241e. The image contains 13317×9578 pixels of 3 m^2 covering $40.0 \times 29.7 \text{ km}^2$ including the regions with no data.

2. OBSERVATIONS

We analyze the images in one scene from the Planet Labs archive with identifier 20220530_173806_19_241e indicating that the observations were made on May 30, 2022 at 17:38:06 UT by the satellite identified as 241e. Each scene in the archive is a data set containing images in each of eight spectral bands as well as a visual composite in RGB (red-green-blue) format. The images were made with a pixel size on the ground (GSD or ground sample distance) of 4.2 m and covering $\sim 37 \times 22 \text{ km}^2$. The scene includes images processed or orthorectified by Planet Labs to a longitude and latitude grid and resampled to 3.0 m. The orthorectified visual image of the area around San Diego, CA is shown in figure 1.

3. CHARACTERISTIC SIGNATURES OF MOVING OBJECTS

3.1. Signature in composite visual images

A detail of the visual image (figure 2) shows an airplane moving on or over the runway at the San Diego International airport. The motion is identified by the appearance of three airplanes each in one of the RGB colors. The separation between these three colored versions of the moving object depends on the time delay in the acquisition of the images and the velocity of the moving object. Objects moving too slowly to appear as separate images, such as the boats in figure 3, show a green leading edge, a blue trailing edge, with red in the middle.



Figure 2. Detail of the composite visual image (figure 1) showing an airplane moving on or over the runway at the San Diego International airport. The image covers 1.13×0.77 km.

3.2. Signature in differenced images

Figure 4 shows the airplane of figure 2 in the eight spectral bands of the SuperDove satellite arranged sequentially in time to show the airplane moving from right to left along the runway. In a differenced image, a moving object appears as a positive and negative pair highlighted against a suppressed background (figure 5). To improve the suppression of the background, the differences are of bands that are adjacent in the spectrum rather than sequential in time. To further suppress the background, the pixels with brightness levels below a 5% threshold are set to zero (figure 6). Difference imaging is commonly used to detect motion in remote sensing, surveillance, computer vision, and astronomy and sophisticated techniques have been developed for different image characteristics (Alard 2000; Bramich et al. 2013). Our differenced images show that a very simple technique is adequate with the different spectral bands of the SuperDove satellite.

4. MILLISECOND TIMING FROM STATIC IMAGES

Planet Labs aims to provide images of the entire land surface of the Earth once per day. The relevant time scale for the acquisition of a single image is on the order of minutes, sufficient to correlate with the illumination angle of the sun and the weather, for example. Furthermore, the images in the archive are mosaics of several camera exposures or frames that were taken at different times as the satellite crossed a region on the ground. The images in the archive do not have exact time stamps but rather the approximate time over which the several images in a mosaic were obtained.



Figure 3. Detail of the composite visual image (figure 1) showing boats moving in the San Diego harbor. The bright green leading edge is a characteristic signature of motion. The image covers 1.31×0.78 km.

In order to measure the velocity of moving objects by comparison of images in different spectral bands, we require the difference in the acquisition time with an accuracy of 1 - 10 ms. This requires an understanding of the imaging process.

The sensor on the SuperDove satellite has 8880×5304 pixels each with a size of $5.5 \times 5.5 \mu\text{m}^2$. In a coordinate system oriented with the orbital track, we label the axes x and y with the satellite moving along the y -axis consistent with the presentation of the “basic analytic” images in the Planet Labs archive. The sensor is covered by a filter with 8 regions of 8880×663 pixels, one for each of the 8 spectral bands. Each individual camera exposure captures these 8 color strips, each covering a different region on the ground.

After a time delay, a second image is taken. This second image is shifted with respect to the first along the ground track of the satellite by the orbital motion. The time delay, set by the maximum frame rate of the camera (~ 0.17 s), is shorter than the time required for one color to exactly overlap another on the ground. Repeated, the process results in a continuous mosaic of partially overlapping images in each color. Where there is overlap, the image-processing pipeline selects one row from the rows of overlapping pixels.

The process is illustrated in figure 7 showing the construction of a mosaic from several strips. From the full image acquired at time, t_0 , extract the color strip for one spectral band to start the mosaic. Repeat for the image acquired at time, t_1 , after the orbit of the satellite has shifted the image on the ground. With a frame rate, $(t_1 - t_0)^{-1}$ rapid enough to provide spatial overlap, align the two overlapping strips and select one of the two overlapping regions. Repeat to fill out the mosaic. Each row of pixels in the mosaic then has the acquisition time of the strip that contributes the row to the mosaic.

Finally, the continuous strip is divided into individual scenes with the same dimensions as the camera sensor. The basic analytic images for one scene in the archive consist of 8 images, one in each of the 8 spectral bands, each with the same number of pixels as the sensor. However, each image is a mosaic of several strips of the same color captured sequentially as the satellite passes over the scene. The identical process operates for each spectral band.

We break the calculation of the acquisition time difference between pixels in the different spectral bands into two steps. In the first step, we find the time difference between the mosaiced images of the eight spectral bands. Because

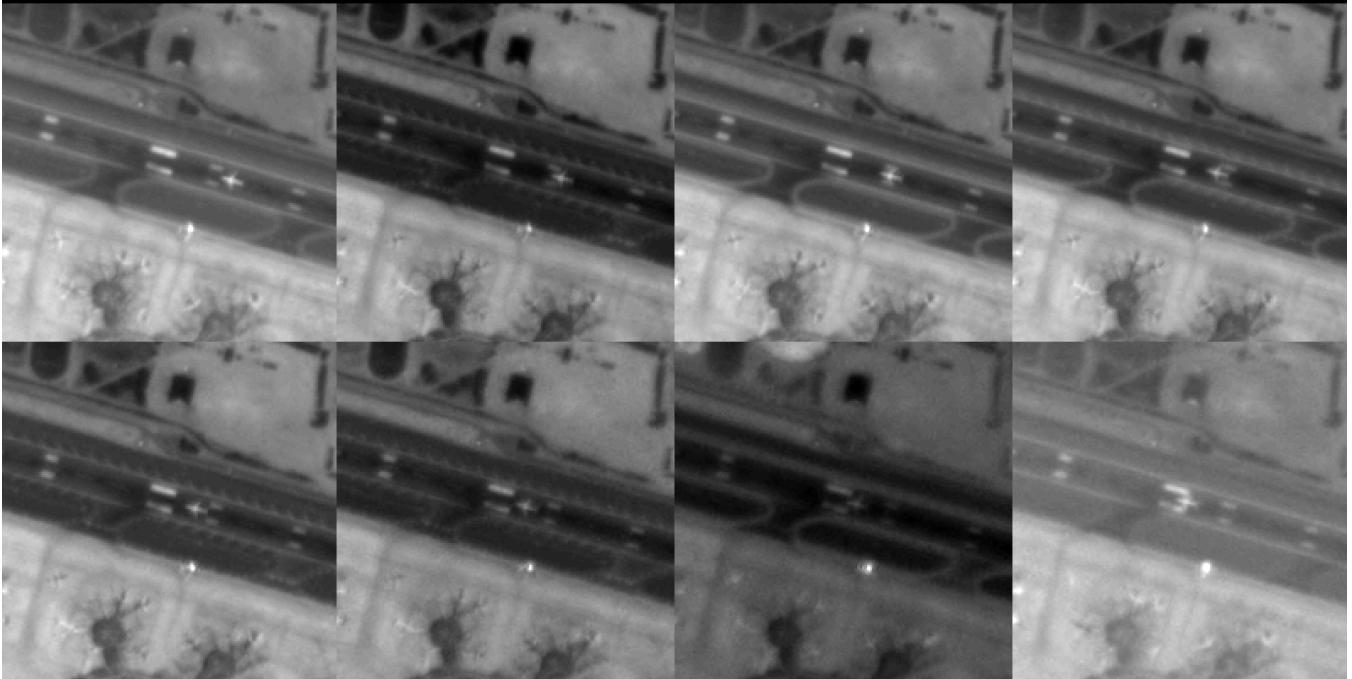


Figure 4. Detail of the full image in eight spectral bands arranged in temporal order: top row, right-to-left, then bottom row, right-to-left. In this temporal order showing the airplane moving west (left), the spectral bands are B, R, G1, G2, Y, RE, NIR, CB (table 1). Each panel covers 0.6×0.6 km.

the progression of acquisition times across the mosaic is set by the frame rate of the camera and the orbital speed of the satellite, the progression is the same for all colors. This defines a single time difference between two images of different colors even though the image of each color includes multiple acquisition times.

This first time difference between spectral bands depends only on the orbital velocity and the sensor dimensions and is given by the width of a color strip on the ground divided by the ground speed of the satellite and the number of color strips on the sensor between the two colors. The ground pixel size or ground sample distance (GSD), defined here as the size of a pixel on the sensor multiplied by the ratio of the altitude of the satellite over the focal length of the camera, is available in the Planet Labs archive for the basic analytic images. The orbital speed of the satellite can be determined from the orbital parameters published in a daily ephemeris for all Planet Labs satellites mainly for the purpose of collision avoidance with other spacecraft. For the purposes of this example, we can assume that the orbit is circular and the Earth is spherical. This allows us to use just one of the published parameters, the mean motion or the number of orbits per day. In this case, the time difference between adjacent colors on the sensor is,

$$\Delta t_{color} = \frac{N_y \mu}{2\pi R_{\oplus} \omega} \quad (1)$$

where $N_y = 663$ is the width in pixels of one color strip, $R_{\oplus} = 6378$ km is the radius of the Earth, μ is the GSD of 4 m, and ω is the mean motion of 15.15 orbits per day. The time difference between colors is $\Delta t_{color} \sim 0.39$ s.

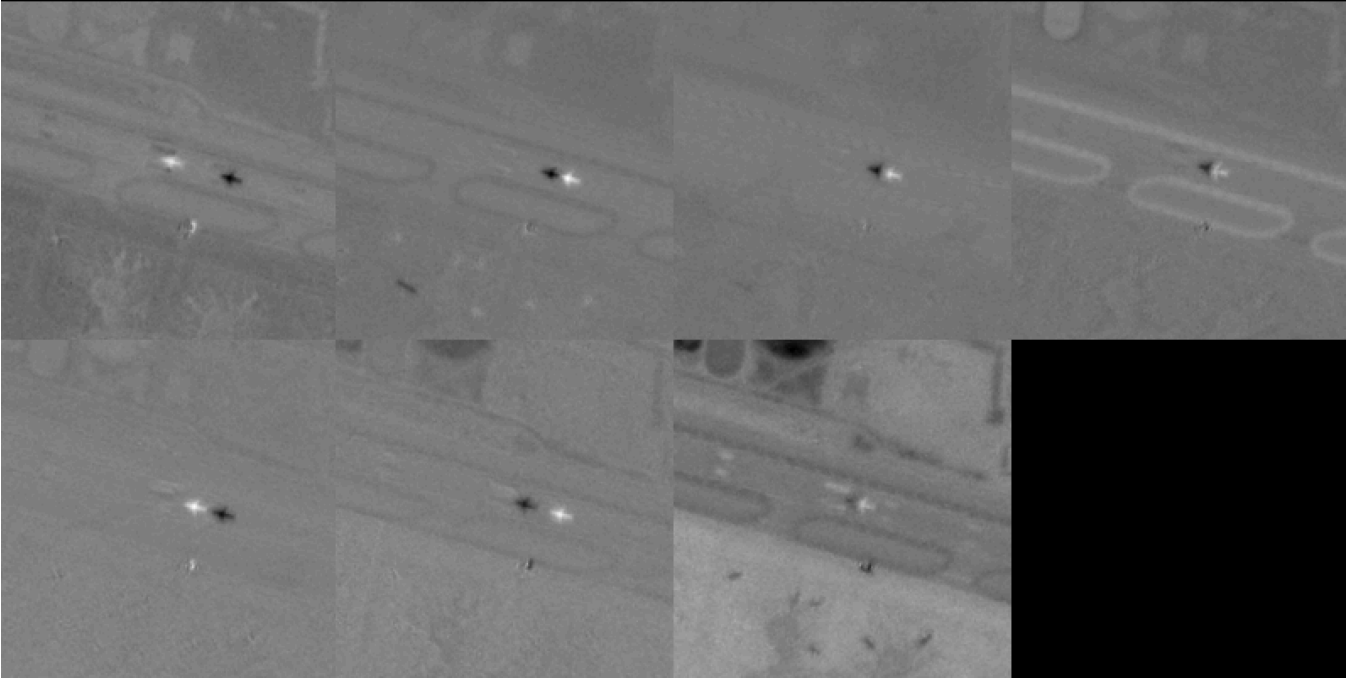


Figure 5. Differences of the images in figure 4 to isolate the moving object. The background is flatter if the images are subtracted in spectral order. Thus the 7 images show the differences CB-B, B-G1, G1-G2, G2-Y, Y-R, R-RE, RE-NIR (table 1). The eighth square (black) has no data.

The second component of the total time difference depends on the location of the object in the mosaiced image of a single color and the progression of acquisition times of the color strips that make up the mosaic. Without the details of the image processing that constructs the mosaic, in particular which of the strips contributes a row of pixels to the full mosaic, we can try to determine the second component from the apparent acceleration of the moving object itself. As a first estimate, we use the time difference between colors to calculate the velocity from the position of the object in all pairs of images in different colors to get a time sequence of velocities. If the object remains in a width where the acquisition time is constant, as would be the case for motion across the satellite track, this estimate of the delay time is correct.

The width of the strip depends on the camera frame rate, the ground velocity of the satellite, and the GSD. For example, if the camera frame rate expressed as an interval is 0.17 s, then the ground motion of the image is 1.2 km between frames, and the pixels within some fraction of this width, depending on the mosaicing pattern, have a constant acquisition time. An object near the boundary of a strip could move into the adjacent strip with a different acquisition time. In this case, the time delay between the positions of the objects needs to be adjusted by the camera frame interval, Δt_{camera} . In general, the measured velocity is,

$$v_i = \frac{\Delta p}{\Delta t_{color} + a} \quad (2)$$

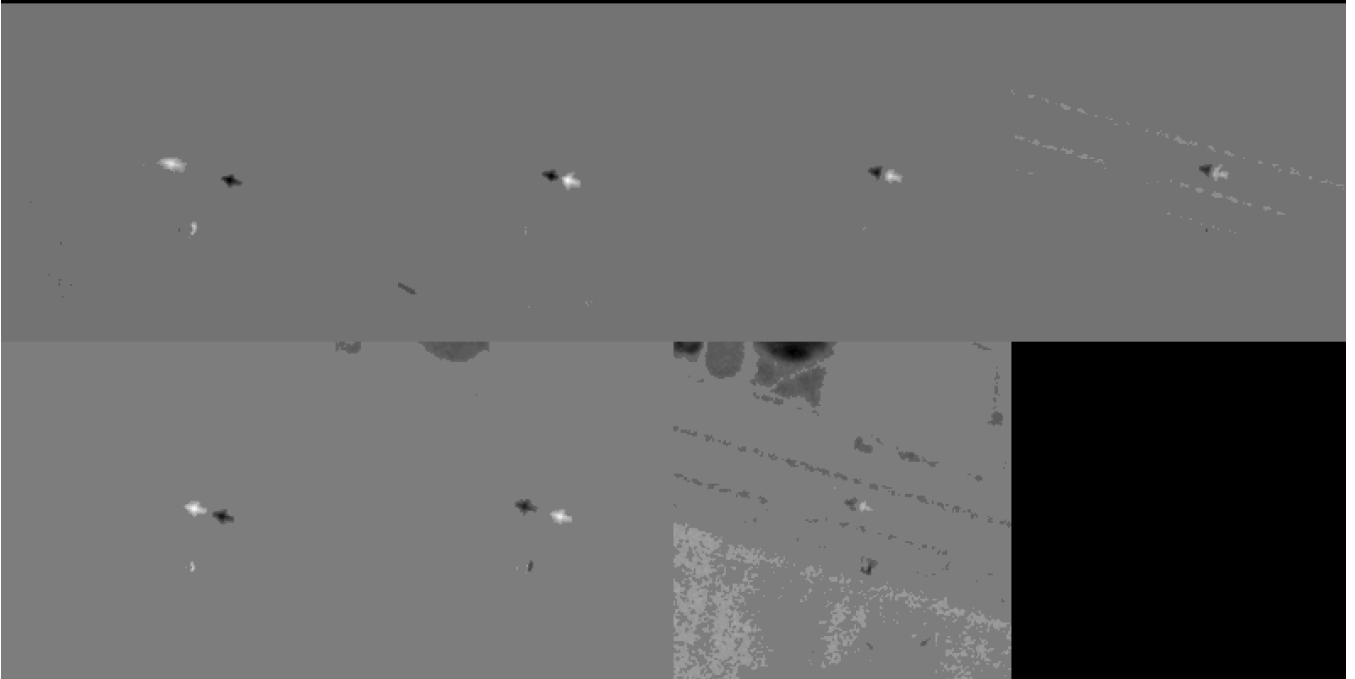


Figure 6. Same as figure 5 after thresholding the images at a constant level based on the histogram of image brightness levels. The same threshold has been applied to all images.

where $\Delta p = p_i(x, y) - p_{i+1}(x, y)$ is the distance between the locations of the object in two color bands, i and $i + 1$. The variable a can take one of 3 values, $0, \pm\Delta t_{camera}$. We can estimate the correct value by minimizing the apparent acceleration between the measured velocities. Since $\Delta t_{color} \sim 2\Delta t_{camera}$, an object crossing a boundary between two acquisition times would appear to change velocity by a factor of about 0.5 or 1.5 compared to the other velocities in the time sequence of velocities in a time interval equal to the first time difference, ~ 0.39 s. For more rapidly moving objects, this is more likely to be due to the difference in acquisition times than the actual acceleration of the object.

5. MEASURING THE VELOCITY

In the first panel in figure 6 showing the thresholded differenced images, the airplane is moving approximately perpendicular to the orbital track and therefore we can use the time delay between colors to estimate the velocity. From equations 1 and 2 and the data for satellite 241e, the time delay is 0.393562 s. The displacement between the positive and negative images of the airplane is 49.6 pixels of 3 m at ground level. The average speed of the airplane in the time between these images is 38.5 ± 5.3 m/s or 86.4 ± 11.8 mph. For reference, the average speed of a Boeing 737 at takeoff is 150 mph.

The error in the measured velocity is dominated by the pixelization and also affected by the ability to define a moving object against a complex background. For objects easily distinguished above the background, the error in location should be a pixel or less. The expected error in the velocity is then about 11 ms^{-1} . The expected error in acceleration from 3 positions would be $\sqrt{3/2}$ larger. We can ignore the error contributed by the smaller uncertainty

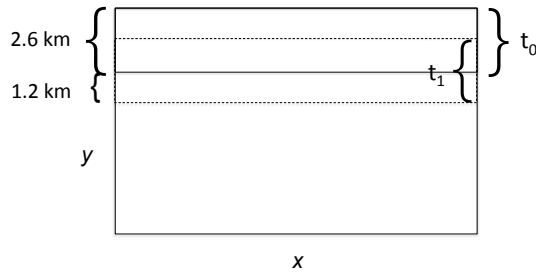


Figure 7. Schematic of the mosaicing process. The large rectangle represents the mosaiced image with a width (dimension in y or vertical) of 20.8 km. The smaller rectangle in solid lines represents the width of one color strip, approximately 2.6 km on the ground, taken at time t_0 . After a delay of one interval of the camera frame rate of 0.17 s, the color strip has moved approximately 1.2 km to the position of the rectangle with dashed horizontal lines. The acquisition time of this strip is t_1 . Depending on the mosaicing pattern, a pixel in the region of overlap may have either acquisition time. The top of the color strip t_0 might not line up with the top of the mosaiced image as suggested in the figure, but the procedure suggested in the text remains valid.

in time. Since the time delay is proportional to square root of the orbital altitude, (\sqrt{r}), the error in the time delay is $\delta r / (2\sqrt{r})$. The expected error in the altitude of a satellite in low earth orbit, δr , described by a two-line element (TLE) model is about 0.1 km (Floher et al. 2008). Thus the fractional error in time is on the order of 0.002.

5.1. Altitude-speed ambiguity

The spatial size of the pixels in the image (GSD) depends linearly on the orbital altitude, ~ 500 km, and the elevation of the Earth’s surface. If the moving object is itself at some altitude above the ground, then the actual distance traveled by the object between images and its velocity will be less than indicated by the number of pixels and the GSD. Since top of the stratosphere is ~ 50 km, the ambiguity results in an uncertainty of less than 10% for objects flying in the atmosphere. Of course, there may be objects moving outside the atmosphere whose speed may be very different from the speed calculated at ground level. Alternatively, stationary objects at altitude may show misaligned colors similar to the signature of motion but due to parallax caused by the spatial alignment which was referenced to the ground in order to eliminate parallax at the ground level. For example, figure 8 shows the apparent ground speed that would be derived for an object that was at altitude and stationary with respect to the Earth’s surface.

$$v_{app} = \frac{h_{obj}}{h_{sat} - h_{obj}} \frac{L}{\Delta t} \quad (3)$$

where h_{obj} and h_{sat} are the respective altitudes of the object and satellite, and L is the linear distance traveled by the satellite in time Δt between images. Clouds at altitude are commonly seen with a signature of motion in Planet Labs images.

In some cases, the altitude-speed ambiguity can be resolved from information in the image itself. For example, if the direction of an object’s motion can be determined, and the object is not moving parallel to the satellite’s orbit, the object’s apparent motion can be resolved into two components: the actual velocity of the object, and an apparent velocity due to the parallax created by the satellite motion (Heiselberg & Heiselberg 2021). The latter allows a determination of the object’s altitude. However, the direction of motion may not be obvious. For example, crosswinds may cause the orientation of an airplane to differ from its direction of motion.

6. CONCLUSIONS AND FUTURE RESEARCH

This research demonstrates at least two characteristic signatures of motion in Earth observation images made with push broom scanning and demonstrates a method for estimating the velocity. The two signatures, different-colored

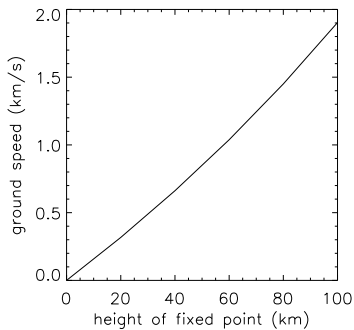


Figure 8. Apparent ground speed (vertical axis) versus altitude (horizontal axis) of an object that is stationary with respect to a location on the Earth’s surface.

ghosts in visual images and positive-negative pairs in the differenced images of individual spectral bands, are distinctive and easy to recognize by eye. We intend to develop software that makes use of pattern-recognition techniques to automatically detect any moving objects in Planet Labs images.

This research is conducted as part of the Galileo Project (Loeb & Laukien 2023) at Harvard University whose goal is to collect scientific quality data that may be useful in the search for objects of extraterrestrial origin (<https://projects.iq.harvard.edu/galileo/home>). For objects within the Earth’s atmosphere, such as those that may be detected in the Planet Labs images, unusual flight patterns have been suggested as an indicator of extraterrestrial origin (Office of the Director of National Intelligence 2021). This research is a first step to develop a method to observe large areas of the Earth, automatically recognize moving objects, and select those whose velocity, acceleration, size or shape fall outside those expected for natural phenomena or common vehicles or projectiles (Watters et al. 2023). Satellite data may also be used with other data in this goal. For example, the Galileo Project is building a network of ground based observatories to collect visual and infrared images of flying objects at much higher spatial resolution than available in satellite images (Szenher et al. 2023). Historical aircraft transponder broadcasts of heading, speed, and altitude are also available to identify common terrestrial aircraft. Historical meteorological data can help identify natural atmospheric phenomena.

¹ We thank Planet Labs for access to data and technical support.

REFERENCES

- Alard, P. 2000, Monthly Notices of the Royal Astronomical Society, 144, 363
- Bramich, D., et al. 2013, Monthly Notices of the Royal Astronomical Society, 428, 2275

Table 1. Spectral Bands of SuperDove Satellites

Color name	Short name	Coverage (nm)	Position
(1)	(2)	(3)	(4)
Coastal Blue	CB	431 - 452	7
Blue	B	465 - 515	0
Green I	G1	513 - 549	2
Green II	G2	547 - 583	3
Yellow	Y	600 - 620	4
Red	R	650 - 680	1
Red-Edge	RE	697 - 713	5
NIR	NIR	845 - 885	6

NOTE—The position refers to the location of the spectral filter with respect to the direction of the satellite. The Blue filter is over the first 663 pixels of the sensor with respect to the satellite motion. Thus the Blue band observes a section of ground ahead of the other bands. Similarly Coastal Blue observes a section of ground behind the other bands. After 8 exposures, a section of ground is observed in all bands.

Easson, G., DeLozier, S., & Momm, H. 2010, *Remote Sensing*, 2, 1331

Floher, T., Krag, H., & Klinkrad, H. 2008, in *Proceeding of the Advanced Maui Optical and Space Surveillance Technologies Conference*, ed. S. Ryan (The Maui Economic Board)

Heiselberg, H. 2019, *Sensors*, 19, 2873

Heiselberg, P., & Heiselberg, H. 2021, *Remote Sensing*, 13, 3016

Loeb, A. A., & Laukien, F. H. 2023, *Journal of Astronomical Instrumentation*, 12, 2340003

Office of the Director of National Intelligence. 2021, *Preliminary Assessment: Unidentified Aerial Phenomena*, <https://www.dni.gov/index.php/newsroom/reports-publications/reports-publications-2021/item/2223-preliminary-assessment-unidentified-aerial-phenomena>, Reports & Publications 2021

Planet Labs Corporation. 2021, *Understanding PlanetScope Instruments*, <https://developers.planet.com/docs/apis/data/sensors/>, Planet Labs Corporation

Szenher, M., Delacroix, A., Keto, E., et al. 2023, *Journal of Astronomical Instrumentation*, 12, 2340002

Watters, W. A., Loeb, A., Laukien, F., et al. 2023, *Journal of Astronomical Instrumentation*, 12, 2340006